Polymer 112 (2017) 61–70

Contents lists available at ScienceDirect

Polymer

journal homepage: www.elsevier.com/locate/polymer

High-strength silk fibroin scaffolds with anisotropic mechanical properties

Berkant Yetiskin, Oguz Okay*

Istanbul Technical University, Department of Chemistry, 34469 Istanbul, Turkey

ARTICLE INFO

Article history:
Received 15 December 2016
Received in revised form
20 January 2017
Accepted 28 January 2017
Available online 31 January 2017

Keywords:
Silk fibroin
Anisotropic properties
Cryogels
Scaffolds
Macroporous structure

ABSTRACT

In contrast to isotropic morphologies of synthetic hydrogels, many biological tissues possess anisotropic hierarchical morphologies leading to extraordinary mechanical properties that cannot be mimicked by synthetic materials. Here, we report preparation of anisotropic silk fibroin cryogels and scaffolds exhibiting a Young's modulus in the range of MPa that sustain up to 20 MPa compressive stresses. The cryogels were prepared by a combined directional freezing – cryogelation process starting from an aqueous 4.2 wt% fibroin solution containing butanediol diglycidyl ether cross-linker and N,N,N′,N′-tetramethylethylenediamine. In the first step, the reactor containing the aqueous solution of fibroin, cross-linker, and TEMED was immersed into liquid nitrogen at a controlled rate to create a directionally frozen ice template. In the second step, cryogelation reactions were conducted in this frozen solution at −18 °C whereby the cryo-concentrated fibroin in the unfrozen microzones of the reaction system forms a 3D fibroin network. The scaffolds exhibit anisotropic microstructure and hence anisotropic mechanical properties, e.g., the Young's modulus is 3.4 ± 0.5 MPa and 0.8 ± 0.3 MPa when measured along the directions parallel and vertical to the freezing direction, respectively. All the cryogels could completely be compressed due to squeezing out of water from their pores. Upon removal of the load, the compressed cryogels immediately recover their original dimensions and mechanical properties by absorbing the released water into their pores.

1. Introduction

Hydrogels are chemically or physically cross-linked polymers absorbing large quantities of water without dissolving [1]. Softness, smartness, high water sorption capacity, and similarity to biological tissues make hydrogels unique soft materials. However, there is still a clear distinction between synthetic hydrogels and biological tissues with regard to the microstructure and structure-related mechanical properties. In contrast to the isotropic morphologies of synthetic hydrogels, many tissues including muscles [2], tendon [3], cartilage [4], intervertebral disc [5], and cornea [6] possess anisotropic hierarchical morphologies leading to extraordinary mechanical properties that cannot be mimicked by synthetic materials. Biocompatible anisotropic hydrogels with a good mechanical performance have a broad range of potential applications in tissue engineering, bioseparation, microfluidics, and organic electronics [7].

To prepare gels with anisotropic properties, several strategies have been presented in the past years including directional freezing [7,8], strain-induced reorientation [9–14], self-assembly [15–17], dielectrophoresis [18], micropatterning [19], and 3D printing [20]. Directional freezing is a simple and promising approach to the preparation of aligned porous materials [7,8]. By this technique, the growth of solvent crystals during freezing of a polymer solution is controlled in one direction, e.g., by immersing the reactor containing the solution into a cold bath at a controlled rate. Uniaxial freezing of the solutions of synthetic and natural polymers such as polyvinyl alcohol (PVA) [21], agar [22], agarose [23], chitosan [24], alginate [25,26], collagen [27], gelatin [28], soy proteins [29], silk fibroin [30,31], or colloidal solutions of polymers and nanoparticles [8], such as PVA and silica in a cold bath followed by removing oriented solvent crystals via freeze-drying produce aligned porous materials with various microstructures. However, such materials generally dissolve in good solvents and exhibit poor mechanical properties due to the absence of chemical cross-links interconnecting the polymer chains or the particles, limiting their application areas. For instance, anisotropic scaffolds based on

* Corresponding author.
E-mail address: okayo@itu.edu.tr (O. Okay).

http://dx.doi.org/10.1016/j.polymer.2017.01.079
0032-3861/

chitosan/alginate produced by directional freezing exhibit a Young's modulus of around 5 kPa [26], while gelatin scaffolds rupture under 0.23 MPa compressive stresses [28]. However, anisotropic scaffolds suitable for tissue engineering applications should sustain high stresses in the order of MPa to protect their integrity.

An alternative strategy is to combine the directional freezing with the cryogelation technique to prepare mechanically strong anisotropic gels. Cryogelation is a simple route to produce 3D highly porous polymer networks of high toughness and superfast responsivity [32,33]. Cryogelation reactions are conducted below the freezing point of the reaction solution, during which the solvent crystals are in equilibrium with the unfrozen liquid microchannels containing cryo-concentrated reactants [32]. Thus, the reactions only proceed in the unfrozen microchannels leading to the formation of macroporous gels with thick pore walls. The combined directional freezing – cryogelation approach was first reported by our group in 2008 to produce butyl rubber (BR) organogels with an aligned porous structure [34]. BR solution in cyclohexane was first directionally frozen below the melting point of the solution and then BR chains are intermolecularly cross-linked in the frozen solution using sulfur monochloride as a cross-linker. The anisotropic BR organogels are very tough and can be compressed up to about 99% strain without any crack development [34]. Several research groups have recently reported the combination of the directional freezing technique with redox-, gamma-, or UV-initiated cross-linking cryopolymerization to prepare hydrogels based on chemically cross-linked poly (meth)acrylates with anisotropic morphologies and mechanical properties [35–40]. For instance, poly (ethylene glycol) diacrylate scaffolds produced by directional freezing – cryopolymerization technique exhibit a Young's modulus of 8 kPa and 80 kPa during compressions along the directions perpendicular and parallel to the freezing direction, respectively [36].

Silk fibroin gels are important materials due to their attractive properties such as a high mechanical strength, biocompatibility, and controlled degradability [41–43]. Gelation of silk fibroin in aqueous solutions mainly occurs by self-assembly of fibroin molecules via intermolecular β-sheet crystallites acting as physical cross-links. The formation of β-sheets and hence fibroin gelation can be induced by several triggers such as pH [44], temperature [45], fibroin concentration [46], cations [47], diepoxide cross-linkers [48], vortexing [49], and electrical field [50]. In tissue engineering applications, a high mechanical strength and an interconnected open pore structure with micrometer-sized pores are essential considerations in the development of silk fibroin gels and scaffolds. In addition, an anisotropic microstructure and anisotropic mechanical properties are also required in fibroin scaffolds to mimic the biological tissues. To our knowledge, there is only one report on the preparation of silk fibroin scaffolds with anisotropic mechanical properties [30]. These scaffolds were prepared by uniaxial freezing of aqueous fibroin solutions followed by freeze-drying to fix the anisotropic microstructure formed due to the ice template. Because the scaffolds are soluble in aqueous environment, they were finally treated with methanol to induce the formation of β-sheets [30]. The scaffolds thus produced exhibit a low mechanical strength, e.g., their Young's modulus is below 4 kPa [30]. This is expected due to the fact that the cross-linking occurs after forming the pore walls of the scaffold leading to the formation of weak intermolecular bonds.

The aim of this study was to prepare high-strength biocompatible scaffolds with anisotropic mechanical properties. Here, we describe preparation of anisotropic silk fibroin cryogels and scaffolds exhibiting a Young's modulus in the range of MPa that sustain up to 20 MPa compressive stresses. The cryogels were prepared by a combined directional freezing – cryogelation process starting from an aqueous 4.2 wt% fibroin solution containing butanediol diglycidyl ether cross-linker and N,N,N′,N′-tetramethylethylenediamine (TEMED). In the first step, the reactor containing the aqueous solution of fibroin, cross-linker, and TEMED was immersed into liquid nitrogen at a controlled rate to create a directionally frozen ice template. In the second step, the cryogelation reactions were conducted in this frozen solution at −18 °C whereby the cryo-concentrated fibroin in the unfrozen microzones of the reaction system forms a 3D fibroin network. The scaffolds exhibit anisotropic microstructure and hence anisotropic mechanical properties, e.g., the Young's modulus is 3.4 ± 0.5 MPa and 0.8 ± 0.3 MPa when measured along the directions parallel and vertical to the freezing direction, respectively. As will be seen below, all the cryogels could completely be compressed due to squeezing out of water from their pores. Upon removal of the load, the compressed cryogels immediately recover their original dimensions and mechanical properties by absorbing the released water into their pores.

2. Experimental section

2.1. Materials

The cross-linker butanediol diglycidyl ether (BDDE, Sigma-Aldrich), N,N,N′,N′-tetramethylethylenediamine (TEMED, Sigma-Aldrich), Na_2CO_3 (Merck), and LiBr (Merck) were used as received. *Bombyx mori* cocoons were purchased from Bursa Association of Agricultural Sales Cooperatives for Silk Cocoons (Kozabirlik, Turkey). Silk fibroin was separated from cocoons by boiling them for 1 h in aqueous solution of 0.02 M Na_2CO_3 to remove the sericin proteins followed by washing the remaining fibroin three times with distilled water at 70 °C, for 20 min each [44]. Silk fibroin was dissolved in aqueous 9.3 M LiBr at 60 °C for ~2 h and then dialyzed using dialysis tubing (10000 MWCO, Snake Skin, Pierce) for 3 days against water that was changed three times a day [44]. After centrifugation, the final concentration of silk fibroin in aqueous solution was about 5 w/w%, which was determined by weighing the remaining solid after drying.

2.2. Preparation of fibroin cryogels

Anisotropic fibroin cryogels were prepared by directional freezing of aqueous 4.2 wt% fibroin solution containing BDDE cross-linker and TEMED (0.25 v/v%) in liquid nitrogen followed by conducting the cryogelation reactions at −18 °C for 24 h. BDDE concentration in the fibroin solution was set to 20 mmol epoxy per gram of fibroin [48]. Typically, 5 mL of 5 wt% fibroin solution were mixed with BDDE (0.50 mL), TEMED (15 μL), and water to make the final volume 6 mL. The homogeneous fibroin solution was then transferred into several 1 mL plastic syringes of 4 mm internal diameter. Each plastic syringe containing the gelation solution was then connected to the upper clamp of the Zwick-Roell test machine, which was moved downward at a constant rate R into a cold bath containing liquid nitrogen. Experimental apparatus for directional freezing of aqueous 4.2 wt% fibroin containing BDDE and TEMED is shown in Fig. 1a. The immersion rate R of the syringes into liquid nitrogen controlled by the software of the test machine was varied between 2.5 and 35 mm min^{-1}. The syringes were then placed in a cryostat at −18 °C to conduct the cryogelation reactions for 1 day. Control experiments were also carried out as described above, except that the directional freezing step was not applied to the fibroin solutions.

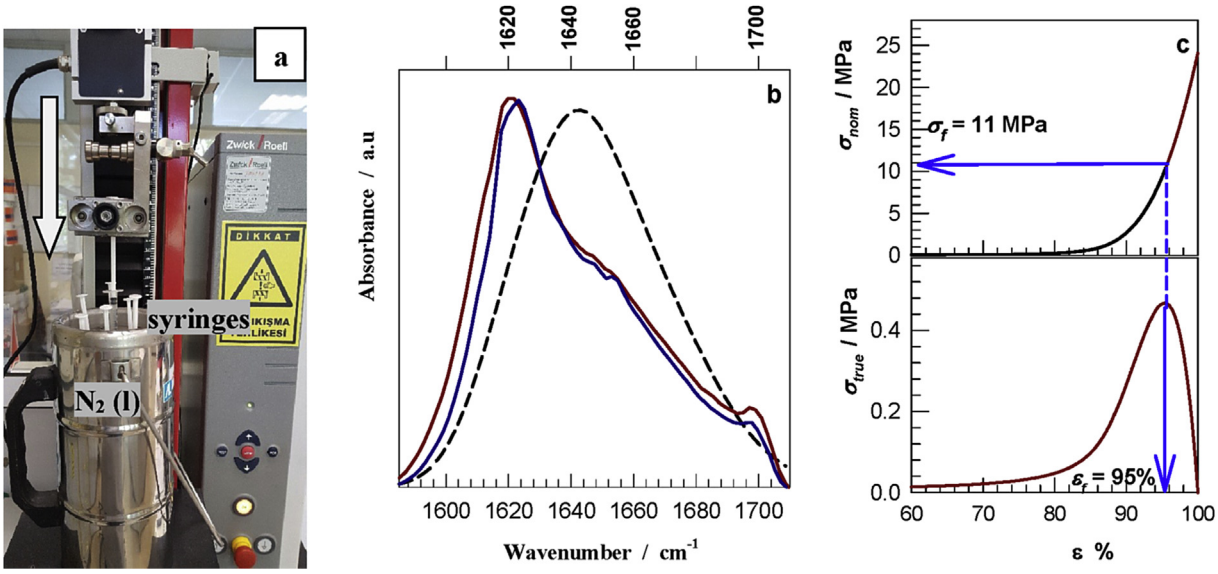

Fig. 1. (A): Experimental apparatus for the directional freezing of aqueous fibroin solutions. The syringes containing aqueous solution of fibroin, BDDE and TEMED are immersed in liquid nitrogen at a controlled rate R before conducting the cryogelation reactions at −18 °C. **(B):** Amide I region of ATR-FTIR spectra of freeze-dried silk fibroin before (dashed curve), and after directional freezing - cryogelation (solid curves) at $R = 2.5$ (dark red) and 35 mm min^{-1} (dark blue). **(C):** Typical stress-strain curves of cryogel samples up to around 99% compressions where the nominal stress σ_{nom} and true stress σ_{true} are plotted against the compressive strain ε. $R = 20$ mm min^{-1}. The samples were compressed parallel to the freezing direction. The blue arrows indicate calculations of the fracture nominal stress σ_f and fracture strain ε_f from the maximum in σ_{true} - λ plot. (For interpretation of the references to colour in this figure legend, the reader is referred to the web version of this article.)

2.3. Swelling and gel fraction measurements

The frozen cryogel samples after preparation were first thawed at room temperature for 30 min and then immersed in a large excess of water for at least 3 days by replacing water several times to extract any soluble species. The swelling equilibrium was tested by weighing the gel samples as well as by measuring the diameter of the gel samples using a calibrated digital compass (Mitutoyo Digimatic Caliper, Series 500, resolution: 0.01 mm). The equilibrium swollen gel samples were taken out of water and immediately frozen at −25 °C for 1 day. The samples were freeze-dried at −40 °C under 0.12 mbar vacuum for 1 day and at −60 °C under 0.011 mbar for an additional 1 day. The freeze-drying system consisted of a freeze-dryer (Christ Alpha 2–4 LD plus) connected to a vacuum pump (Vacuubrand RZ 6). The pressure during freeze-drying was adjusted using a valve controller and monitored by an active digital controller. All cryogel samples were freeze-dried under the same conditions. The equilibrium weight q_w and volume swelling ratios q_v were calculated as $q_w = m/m_{dry}$ and $q_v = (D/D_{dry})^3$, respectively, where m and D are the mass and the diameter of the equilibrium swollen gel sample, respectively, and m_{dry} and D_{dry} are the same quantities for the freeze-dried sample. The gel fraction W_g, that is, the conversion of fibroin to the 3D fibroin network (mass of water-insoluble fibroin/initial mass of the fibroin in the feed) was calculated from the masses of dry fibroin network and from the fibroin in the feed.

2.4. ATR-FTIR measurements

Fourier-transform infrared (FTIR) spectra of the freeze-dried samples were obtained using a single bounce diamond attenuated total refractance (ATR) module on a FTIR spectrometer (Nicolet Nexus 6700) equipped with a liquid nitrogen cooled mercury-cadmium-telluride (MCT) detector. The resolution of each spectrum was 4 cm^{-1}, and 64 interferograms were coadded in the range of 500–4000 cm^{-1}. The dashed and solid curves in Fig. 1b present the Amide I band region (1580–1720 cm^{-1}) of FTIR spectra of freeze-dried fibroin before and after directional freezing - cryogelation, respectively. The peak at 1640 cm^{-1} corresponding to the random coil conformation disappears after cryogelation and a new peak at 1620 cm^{-1} appears which was assigned to β-sheet conformation [51,52]. In addition to this peak, shoulders at 1660 and 1698 cm^{-1} are seen after cryogelation, which were assigned to the α-helix and β-turn conformations, respectively. To estimate the conformation of fibroin, FTIR spectra of the samples were analyzed using PeakFit software (Version 4.12, SeaSolve Software Inc.). Linear baseline correction was applied to the Amide I region before the band was deconvolved by Gauss Amplitude function [48]. For the curve fitting procedure, the initial band positions at 1620, 1640, 1660, and 1698 cm^{-1}, representing β-sheet, random coil, α-helix, and β-turn conformations, respectively, were fixed, allowing their widths and heights to vary (Fig. S1).

2.5. Mechanical tests

Uniaxial compression measurements were conducted on cryogel samples both in equilibrium swollen and dried states. The samples were cut from the directions parallel and vertical to the freezing direction to obtain a rectangular shape of dimensions 33 ± 6 mm × 32 ± 4 mm × 2.2 ± 0.4 mm. The compression tests were performed at 23 ± 2 °C on a Zwick Roell test machine using a 500 N load cell [53]. An initial compressive contact to 0.05 N was applied to ensure a complete contact between the sample and the surface. Load and displacement data were collected during the experiments at a constant crosshead speed of 0.3 mm min^{-1}. Compressive stress was presented by its nominal σ_{nom} and true values σ_{true}, which are the force per cross-sectional area of the undeformed and deformed specimen, respectively. Assuming the sample volume remains constant during deformation, the true stress σ_{true} was calculated as $\sigma_{true} = \lambda\ \sigma_{nom}$ where λ is the deformation ratio (deformed length/original length). The compressive strain is given by the compression ratio ε which is the change in the sample length relative to its initial length, i.e., $\varepsilon = 1 - \lambda$. Fig. 1c shows typical stress-strain curves of fibroin cryogels, where the nominal

σ_{nom} and true stresses σ_{true} are plotted against the strain ε. It is seen that although σ_{nom} increases continuously with increasing strain up to about 99% compression, the corresponding σ_{true} - λ plot passes through a maximum revealing the onset of a failure in the cryogel specimen [53]. Therefore, the fracture nominal stress σ_f and the fracture strain ε_f were calculated from the maxima in σ_{true} - λ plots, as indicated by the blue arrows in the figure. The compression modulus E was calculated from the slope of stress-strain curves between 2 and 4% compressions while the stress at 3% compression was reported as the compressive stress σ_{comp}. For reproducibility, at least six samples were measured for each sample and the results were averaged.

2.6. Texture determination

Cross-sectional scanning electron microscopy (SEM) studies were performed on freeze-dried cryogel samples at various magnifications between 20 and 1000 times in a field emission scanning electron microscope (JEOL JSM-6510LV). All samples were coated with gold for 3 min using a Sputter coater (S150 B Edwards) prior to the measurements. Texture determination of the freeze-dried and swollen cryogel samples was also carried out using an image analyzing system consisting of a microscope (XSZ single Zoom microscope), a CDD digital camera (TK 1381EG) and a PC with the data analyzing system Image-Pro Plus. For this purpose, cylindrical gel samples of 3.7 mm in diameter were cut into thin slices of about 1 mm in thickness. The measurements were conducted at magnifications between 10 and 100 times.

3. Results and discussion

Anisotropic silk fibroin scaffolds were prepared by lowering the reactor containing an aqueous solution of fibroin, BDDE cross-linker, and TEMED into liquid nitrogen at a controlled rate followed by conducting the cryogelation reactions at −18 °C for 24 h (Fig. 1a). The immersion rate R of the gelation solution into liquid nitrogen was varied between 2.5 and 35 mm min^{-1}. In control experiments, cryogelation reactions were conducted without the immersion period, i.e., by cooling the solution from 23 ± 2 to −18 °C and keeping at this temperature for 24 h to obtain isotropic cryogels.

Fig. 2a shows the equilibrium weight q_w and volume swelling ratios q_v of the cryogels and the gel fraction W_g plotted against the immersion rate R. The data for isotropic cryogels are shown at $R = 0$, as indicated by an arrow. The gel fraction W_g representing the conversion of water-soluble fibroin to a 3D fibroin network is 1.3 ± 0.2 indicating a complete conversion, and the presence of bound water that cannot be separated by freeze-drying [54]. As detailed before [48,55], BDDE reacts with the amino groups on fibroin to form intermolecular cross-links, whereby the mobility of fibroin molecules significantly reduces triggering the conformational transition in fibroin from random coil to β-sheet structure. The insolubility of fibroin after the directional freezing - cryogelation process also suggests formation of β-sheet crystallites acting as interstrand cross-links. Indeed, the results of β-sheet contents estimated from the analysis of the Amide I band region of FTIR spectra show that fibroin chains before gelation have 12 ± 2% β-sheet structures, while their contribution increases to 28 ± 1 and 31 ± 2% in isotropic and anisotropic cryogels, respectively (Fig. S2). The higher β-sheet content of anisotropic cryogels as compared to the isotropic ones indicates that freezing in liquid nitrogen before cryogelation promotes β-sheet crystallization. Fig. 2a also reveals that both the weight q_w and volume swelling ratio q_v of anisotropic cryogels are independent on R and they equal to 12.3 ± 0.4 and 1.2 ± 0.1, respectively. Isotropic cryogels exhibit a slightly higher degree of swelling and a gel fraction W_g of 1.1 ± 0.1 indicating that the immersion period increases the amount of bound water in the cryogels.

The fact that the mass of the cryogels 12-fold increases upon swelling in water while their volume remains almost constant suggests that the swelling process of the cryogels is mainly governed by filling of their pores with water [56]. Assuming the pore volume remains constant during swelling, the total porosity P can be estimated from the weight and volume swelling ratios using the equation [56]: $P = 1 - q_v[1 + (q_w - 1)\,\rho]^{-1}$ where ρ is the fibroin density (1.35 g/mL) [57]. Calculations show that the porosity P of

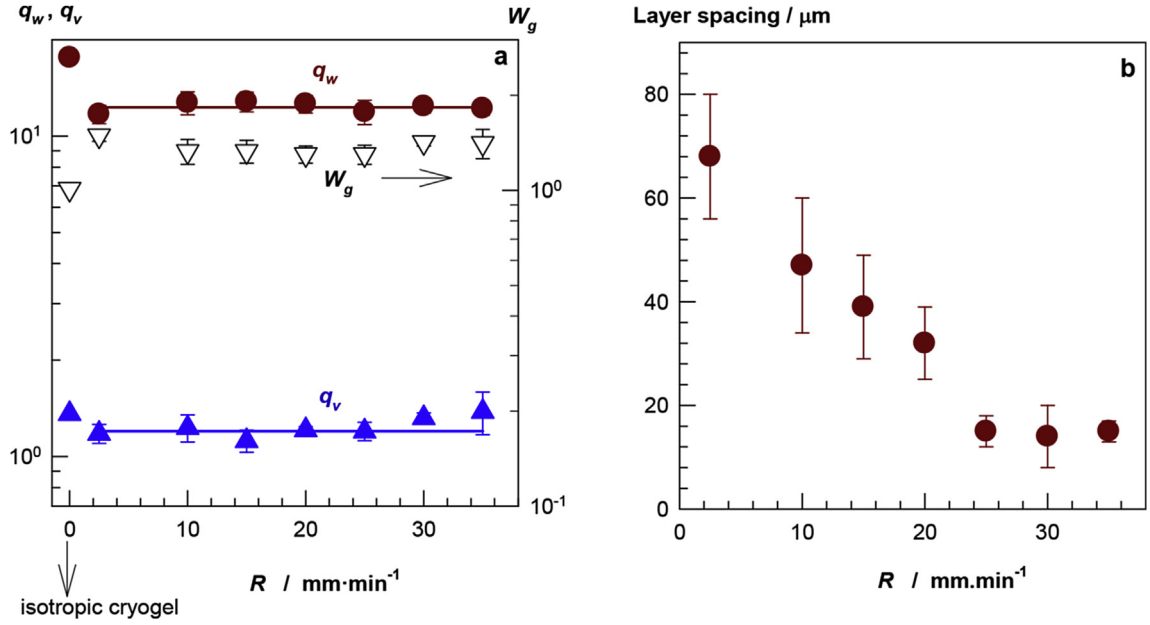

Fig. 2. (A) The gel fraction W_g (open symbols), equilibrium weight q_w (filled circles) and volume swelling ratios q_v of the cryogels (filled triangles) shown as a function of the immersion rate R. The data at zero immersion rate are for isotropic cryogels. **(B)** Spacing between fibroin layers, i.e., channel width in anisotropic cryogel scaffolds shown as a function of R.

both isotropic and anisotropic cryogels is 93 ± 1% indicating their highly porous structure. Indeed, cross-sectional optical images of isotropic and anisotropic cryogel samples shown in Fig. 3a and 3b–d, respectively, reveal existence of micrometer-sized pores. The isotropic cryogel has a disordered pore structure within an interconnected 3D fibroin network while all cryogels prepared after directional freezing – cryogelation process possess long aligned fibroin layers interconnected with fibroin branches forming a 3D network containing macropores. The images in Fig. 3b–d also show that increasing immersion rate R of the reaction solution into liquid nitrogen prior cryogelation decreases the spacing between the fibroin layers, i.e., the width of microchannels.

Fig. 4a and b shows typical scanning electron micrographs of cross-sections of isotropic (a) and anisotropic cryogel scaffolds formed at $R = 30$ mm min^{-1} (b). Isotropic cryogel sample consists of randomly oriented spherical and ovaloid pores of 30 ± 11 μm in diameter while the anisotropic sample possesses several hundred micrometers long, aligned fibroin layers producing a channel-like porous structure. The fibroin layers are interconnected by perpendicularly oriented branches to form a "fishbone" morphology. We have to mention that all the SEM and optical images presented here are cross-sectional views of the scaffolds and therefore, the aligned layers and channels are perpendicularly oriented to the immersion direction. For instance, Fig. 4c and d showing SEM images of the cryogels formed at $R = 20$ and 25 mm min^{-1}, respectively, at a low magnification reveals radially oriented pore structure of the scaffolds. These results suggest that the growth of ice crystals occurs from the surface of the syringes which is in conduct with the cooling liquid at −196 °C to its interior rather than in the direction in which the syringe is lowered into liquid nitrogen. A similar observation was recently reported by Arrua and Hilder in the preparation of cross-linked polyacrylates by directional freezing and photoinitiated cryocopolymerization [39]. We attribute the directional freezing in radial direction to the higher effective thermal conductivity in radial direction as compared to the longitudinal (immersion) direction because the heat flux must travel a shorter path in the former direction.

Fig. 5 shows a scheme representing the unidirectional growth of ice crystals and formation of fibroin layers interconnected by branches. The temperature gradient in the fibroin solution induced by the contact with liquid nitrogen results in growing of ice from the surface of the cylindrical reactor toward the center. As water freezes, fibroin molecules together with BDDE cross-linker and TEMED are expelled from the formed ice crystals and accumulate around the growing crystals to form unfrozen domains of the reaction system. Thus, in addition of the temperature gradient, a concentration gradient is established across the moving freezing front due to the cryo-concentration of the reactants. This causes Mullins-Sekerka instability leading to the collapse of the moving freezing front leaving behind pockets of unfrozen concentrated fibroin solution [7,8,58]. After the cryogelation reactions at −18 °C, the cryo-concentrated unfrozen fibroin solution between the aligned ice crystals turns to a dense gel making the fibroin layers and branches while ice act as template to form pores after thawing and freeze-drying. The primary periodicity of the aligned porous structures is defined by the Mulling-Sekerka instability wavelength [58]. This wavelength is determined by competition between the destabilizing solute interfacial concentration gradient and the stabilizing effects acting to preserve the planarity of the interface, e.g., the imposed temperature gradient and surface energy of the solid/liquid interface [58]. The layer spacing, i.e., the channel diameter of 14 ± 7 μm in Fig. 4b well compares with the instability wavelength of 15 μm for aqueous PVA solutions [8].

The results also show that the spacing between the fibroin layers strongly depends on the immersion rate R. Fig. 6 showing SEM images of fibroin scaffolds formed at various R between 2.5 and 35 mm min^{-1} indicate that the layer spacing is inversely proportional to the immersion rate. The average spacing between the layers were calculated by analyzing SEM images at various magnifications. The results are collected in Fig. 2b where the layer spacing is plotted against R. At low immersion rates R, the layer spacing approaches to 70 μm with a broad length distribution while at $R > 20$ mm min^{-1}, it is rather uniform and around 15 μm. Decreasing layer spacing with increasing immersion rate is due to the simultaneous increase of the freezing rate leading to the formation of a larger number of growing ice crystals [32]. Some internal microcracks were also observed in the cryogel samples formed at high immersion rates (≥25 mm min^{-1}) which we attribute to rapid cooling of the fibroin solution (Fig. S3).

Anisotropic microstructure of the cryogels resulted in anisotropic mechanical properties, as demonstrated by uniaxial compression tests. The tests were performed by cutting dry and swollen cryogel specimens from the directions parallel and vertical to the freezing direction and compressing them at a constant speed up to complete compression. Fig. 7 shows stress-strain curves of the cryogel scaffolds formed at various R where the nominal stress σ_{nom}

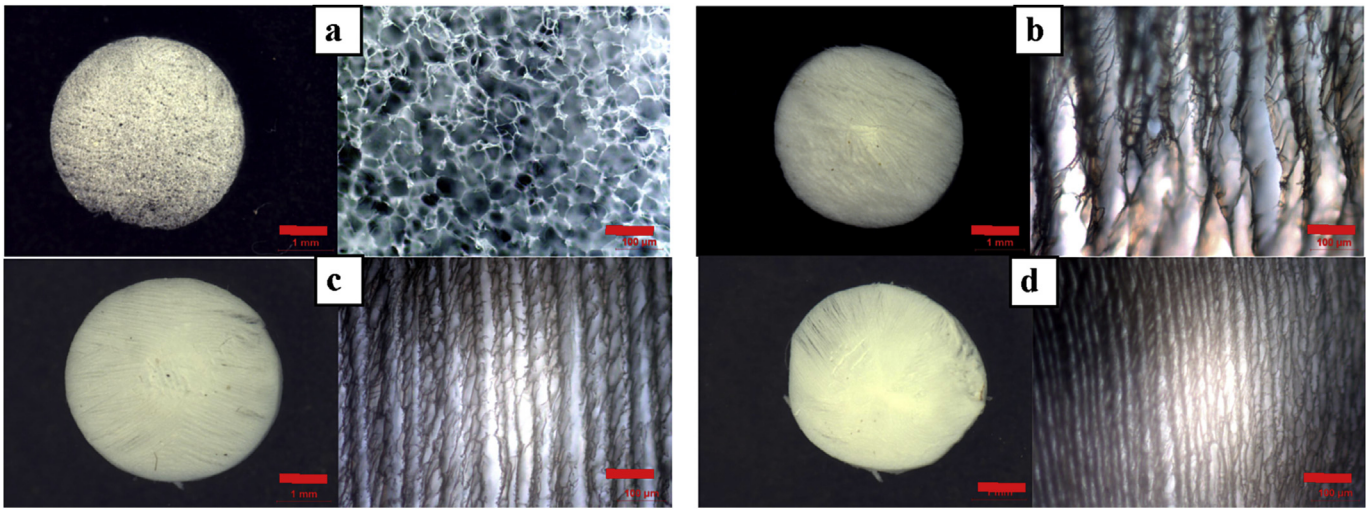

Fig. 3. Optical images of isotropic (a) and anisotropic fibroin cryogels (b–d). $R = 10$ (b), 25 (c), and 35 mm min^{-1}. Scaling bars in 3a–d are 1 mm (left) and 100 μm (right).

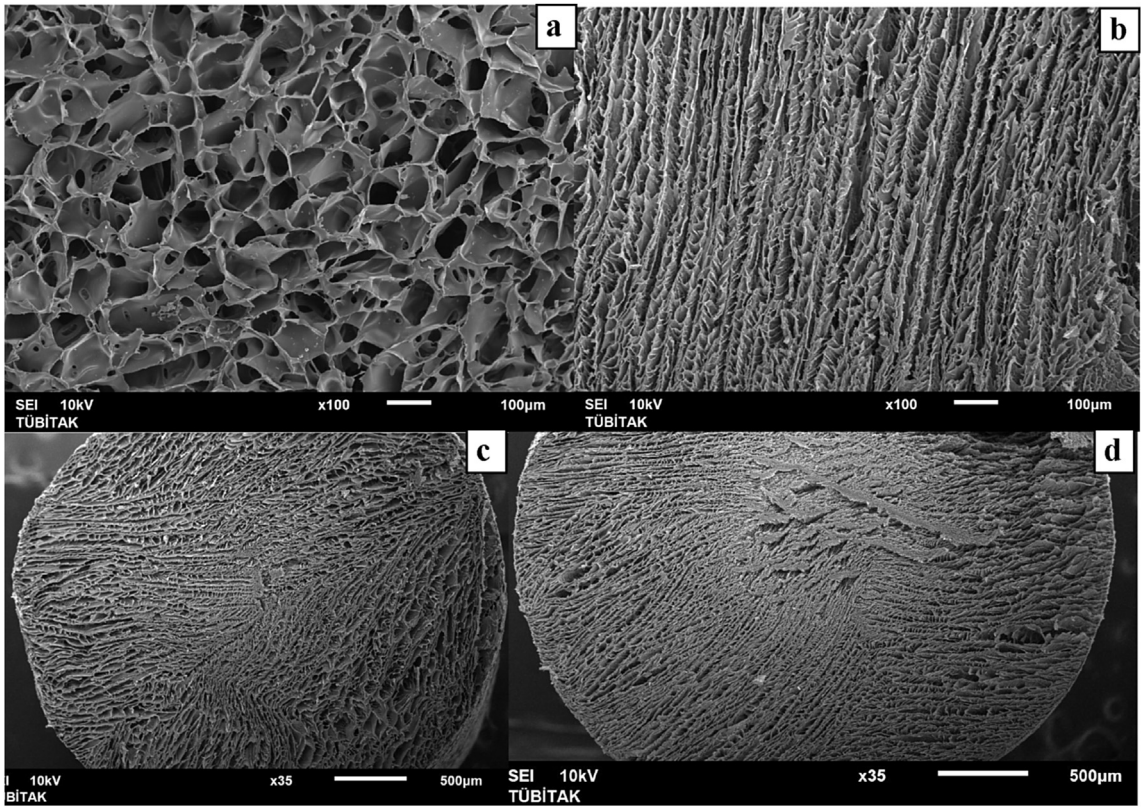

Fig. 4. SEM images of isotropic (a) and anisotropic cryogel scaffolds (b–d). Scaling bars are100 µm (a, b) and 500 µm (c, d). R = 20 (c), 25 (d), and 30 mm min^{-1} (b).

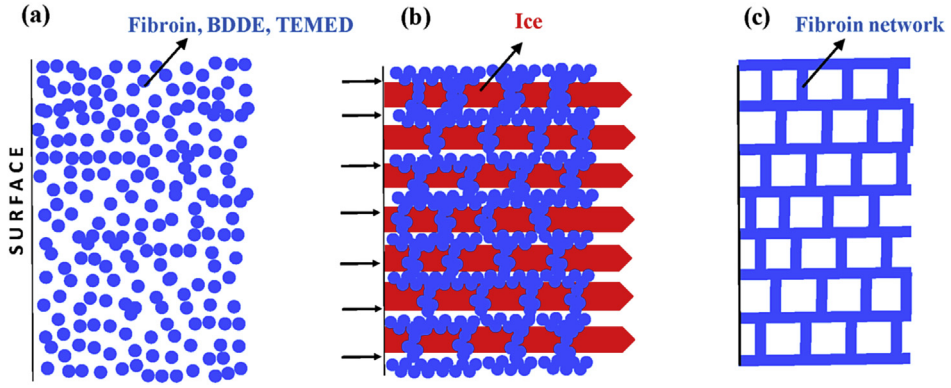

Fig. 5. Cartoon representing formation of aligned porous structure in fibroin cryogels under directional freezing. Fibroin solution before (a) and after directional freezing (b), and after cryogelation (c) is presented.

is plotted against the deformation ε. Note that the curves were corrected by considering the onset of microcracks in true stress σ_{true} – ε plots as detailed in the experimental section and in Fig. 1c. Solid and dashed curves represent the results of the measurements along the directions parallel and vertical to the freezing direction, respectively. The insets show the portion of the curves below σ_{nom} = 0.6 MPa. The cryogels sustain up to ~90% compression at ~20 MPa compressive stresses. This extraordinary mechanical strength is due to the cryo-concentration of fibroin producing dense pore walls of high fibroin concentration [32,33]. For instance, freezing of an aqueous 6 wt% fibroin at −18 °C results in a frozen system composed of 88% ice and the rest being a concentrated unfrozen solution containing 37 wt% fibroin, which is about 6-fold larger than the nominal fibroin concentration [55]. Fig. 7 also shows that, at below R = 30 mm min^{-1}, the initial slope of stress-strain curves corresponding to the Young's modulus E is higher in parallel direction as compared to the vertical direction. Another point is the appearance of a near-plateau regime at around 5% compression in parallel direction during which the scaffolds easily deform under force. As reported before [55], the appearance of a plateau regime indicates that the porous structure is mechanically stable up to the onset of the plateau while it starts to collapse with the onset of the plateau. The results reveal higher mechanical stability of 3D porous structure during compression in parallel direction as compared vertical direction.

The mechanical properties of the cryogels are compiled in Fig. 8 where the Young's modulus E, compressive σ_{comp} and fracture stresses σ_f of dry (left panel) and swollen cryogels (right panel) are

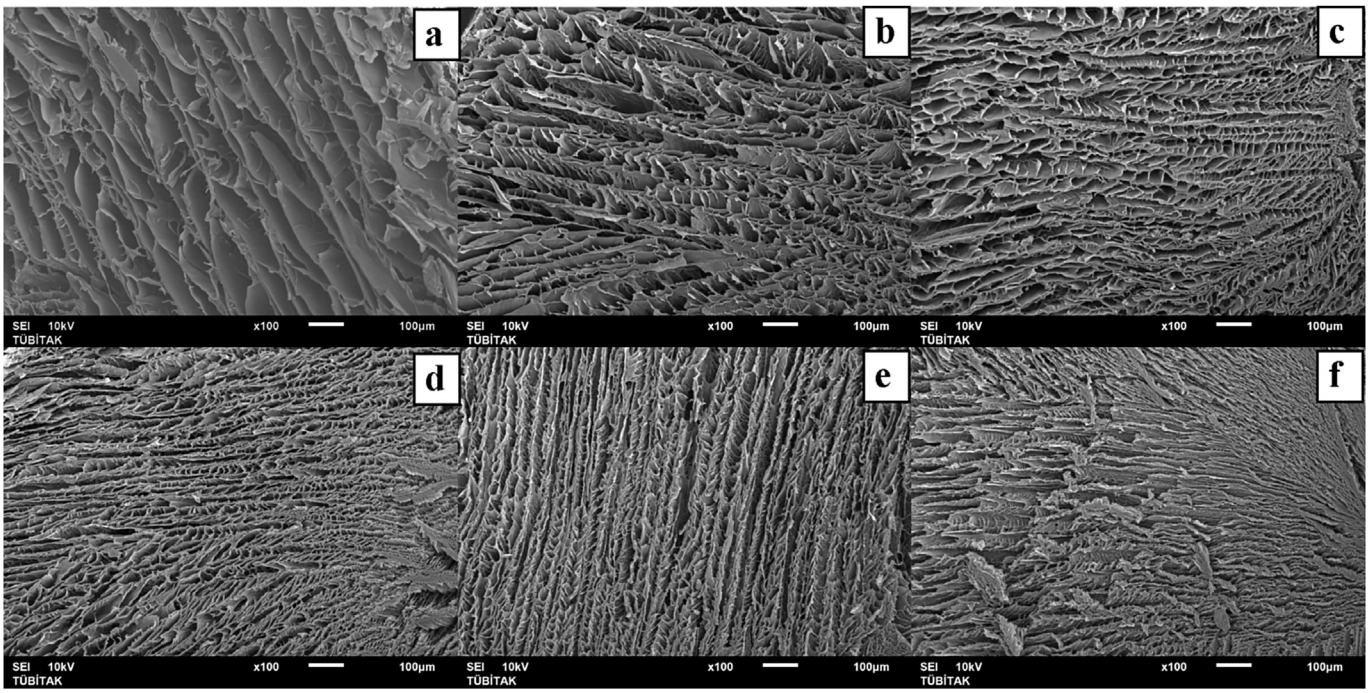

Fig. 6. SEM images of anisotropic cryogel scaffolds. $R = 2.5$ (a), 10 (b), 20 (c), 25 (d), 30 (e), and 35 mm min^{-1} (f). Scaling bars = 100 μm (Magnification = ×100).

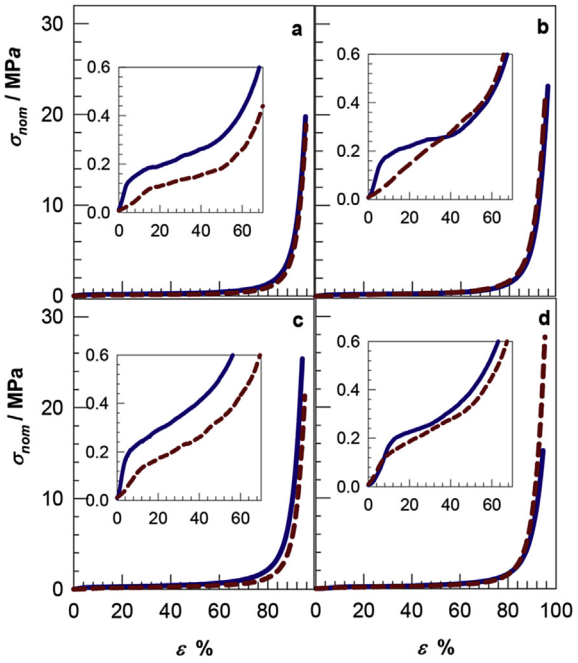

Fig. 7. Stress − strain curves of fibroin scaffolds as the dependence of the nominal stress σ_{nom} on the compressive strain ε. The measurements were conducted parallel (solid curves) and vertical to the freezing direction (dashed curves). Immersion rate = 10 (a), 15 (b), 20 (c), and 30 mm min^{-1} (d).

plotted against the immersion rate R. The circles and triangles represent the data obtained from parallel and vertical directions, respectively. Moreover, the data of isotropic cryogels in both directions shown at $R = 0$ are presented by the filled and open squares. For both dry and swollen cryogel samples, the extent of anisotropy first increases with increasing immersion rate R up to 20 mm min^{-1} and then decreases again with a further increase in R. The modulus E of scaffolds in parallel direction attains a maximum value of 3.4 ± 0.5 MPa at $R = 20$ mm min^{-1}, which is about four-fold larger than that measured in perpendicular direction (0.8 ± 0.3 MPa). Considering the Young's modulus of human cornea is around 3 and 1 MPa in horizontal and vertical directions, respectively [6], the results show that the cryogel scaffolds formed at 20 mm min^{-1} possess a comparable modulus.

The results also show that the anisotropic pore structure of the scaffolds mainly affect the initial part of the stress-strain curves represented by the modulus E and the compressive stress σ_{comp} at 3% compression while the ultimate properties such as the fracture stress σ_f and fracture strain remain unaffected. This could be explained by considering the microstructure of anisotropic cryogels (Figs. 3, 4 and 6): Compressing in parallel to the freezing direction means vertically compressing several hundred nanometers long, radially oriented fibroin layers while, in vertical direction, the branches between the layers are compressed, which are only tens of nanometers. Thus, a much larger stress is initially required to compress the fibroin layers as compared to their branches. As the strain is increased, the porous structure starts to collapse resulting in a decrease of the channel width so that the stress required to deform the cryogel becomes independent of direction. The results also show that all anisotropic scaffolds formed at $R \leq 20$ mm min^{-1} sustain at least 20 MPa compressive stresses as compared to 8 ± 1 MPa for the isotropic scaffold (Fig. 8). The results of swollen cryogels shown in the right panel of Fig. 8 reveals that the modulus, compressive and fracture stresses of the cryogels decrease by one order of magnitude after swelling in water.

The key advantage of the present directional freezing - cryogelation process is the shape and mechanical property recoverability of anisotropic cryogels subjected to complete compressions. This is presented in Fig. 9a and b showing successive compression test results conducted up to about 99% compression. Here, the solid curves show stress-strain curves of cryogel samples prepared at $R = 20$ mm min^{-1} as the dependences of the nominal σ_{nom} and true stresses σ_{true} on the compressive strain ε, respectively. The cryogel samples were compressed parallel (left panel) and vertical to the

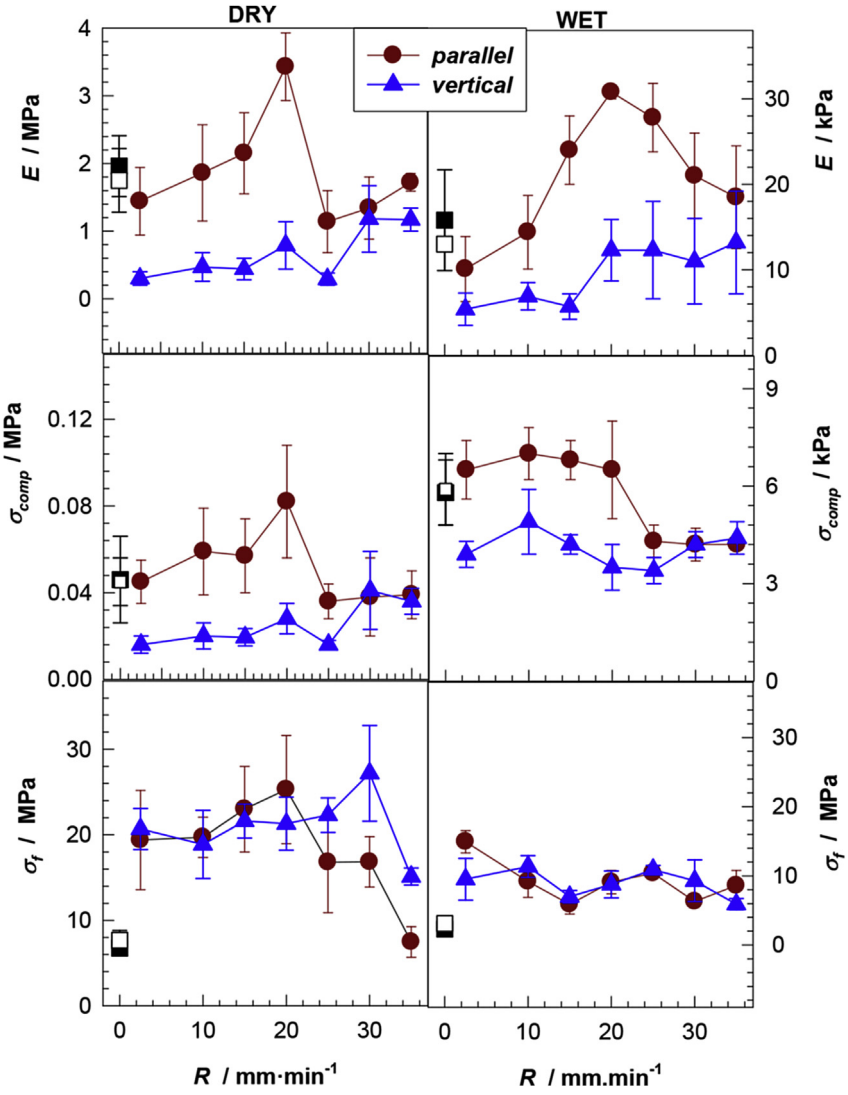

Fig. 8. The compressive modulus E, compressive σ_{comp} and fracture stresses σ_f of dry (left panel) and swollen cryogels (right panel) plotted against the immersion rate. The circles and triangles represent the data obtained from parallel and perpendicular directions, respectively, while the data of isotropic cryogels in both directions are shown by the filled and open squares.

freezing direction (right panel). It is seen that, although the cryogel sample could completely be compressed, a maximum in σ_{true} vs ε plot appears at 95% compression suggesting the formation of microcracks in the sample. After this compression test, the cryogel sample remained in a compressed state due to squeezing out of water from its pores, as seen in the images in Fig. 9c (c1→c3). After release of the piston, the compressed sample absorbs the released water (c3→c5) while adding water completely recovers its original dimension by sucking up water in its pores (c6), so that it can be subjected to the next compression test (see also: Supporting Information Movie). Dashed and dash-dot curves in Fig. 9a and b represent 2nd to 4th compression test results, each conducted after adding water to the gel sample. The insets to the figures reveal a good superposition of the successive stress-strain curves demonstrating that the damage in the cryogel is self-healed upon removing the stress. The average compression at break and fracture stress of four successive tests are 94 ± 1% and 8.4 ± 1.4 MPa, respectively. Similar results were also obtained for isotropic and anisotropic cryogels formed at various immersion rates. Thus, all fibroin cryogels can be compressed up to about 99% strain without any permanent failure.

Supplementary data related to this article can be found online at http://dx.doi.org/10.1016/j.polymer.2017.01.079.

4. Conclusions

Silk fibroin cryogels and scaffolds with anisotropic microstructures and anisotropic mechanical properties could be obtained by a combined directional freezing – cryogelation technique starting from aqueous 4.2 wt% fibroin solutions containing BDDE cross-linker and TEMED. In the first step, the reactor containing the aqueous solution of fibroin, cross-linker, and TEMED was immersed into liquid nitrogen at a controlled rate to create a directionally frozen ice template. In the second step, the cryogelation reactions were conducted in this frozen solution at −18 °C whereby the cryo-concentrated fibroin in the unfrozen microzones of the reaction system forms a 3D fibroin network. The scaffolds exhibit a Young's modulus in the range of MPa and sustain up to 20 MPa compressive stresses. In addition to high mechanical strength, they also exhibit anisotropic microstructure and hence anisotropic mechanical properties, e.g., the Young's modulus is 3.4 ± 0.5 MPa and 0.8 ± 0.3 MPa when measured along the directions parallel and

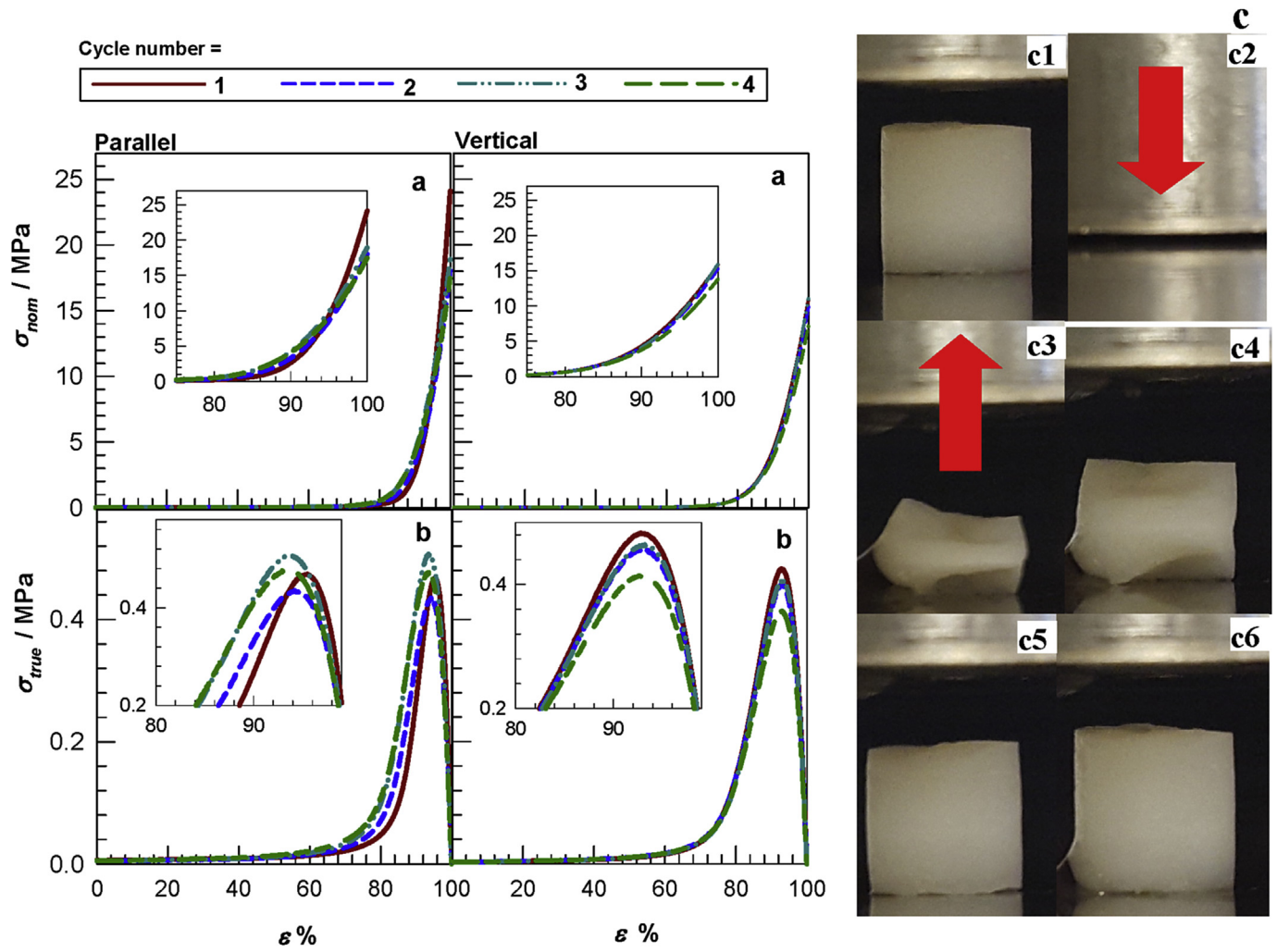

Fig. 9. **(A, B)** Four successive compression test results conducted on anisotropic cryogel samples up to around 99% compression where σ_{nom} (a) and σ_{true} (b) are plotted against the strain ε. The gel samples were prepared parallel (left) and perpendicular to the freezing direction (right). $R = 20$ mm min^{-1}. **(C)** Images showing the initial dimension of the cryogel sample (c1), its compressed state (c2), and the recovery of the initial dimension after release of the piston (c2→c5), and after adding water (c6).

vertical to the freezing direction, respectively. All the cryogels could completely be compressed due to squeezing out of water from their pores. Upon removal of the load, the compressed cryogels immediately recover their original dimensions and mechanical properties by absorbing the released water into their pores. Because many biological tissues possess anisotropic hierarchical morphologies, high-strength anisotropic fibroin cryogels and scaffolds presented here have a broad range of potential applications in tissue engineering, bioseparation, microfluidics, and organic electronics.

Acknowledgments

This work was supported by the Scientific and Technical Research Council of Turkey (TUBITAK), KBAG 114Z312. OO thanks the Turkish Academy of Sciences for the partial support.

Appendix A. Supplementary data

Supplementary data related to this article can be found at http://dx.doi.org/10.1016/j.polymer.2017.01.079.

References

[1] O. Okay, General properties of hydrogels, in: G. Gerlach, K.F. Arndt (Eds.), Hydrogel Sensors and Actuators. Springer Series on Chemical Sensors and Biosensors vol. 6, Springer Berlin Heidelberg, 2009, pp. 1–14.
[2] A.C. Ahn, T.J. Kaptchuk, Spatial anisotropy analyses of subcutaneous tissue layer: potential insights into its biomechanical characteristics, J. Anat. 219 (2011) 515–524.
[3] L.N. Williams, S.H. Elder, J.L. Bouvard, M.F. Horstemeyer, The anisotropic compressive mechanical properties of the rabbit patellar tendon, Biorheology 45 (2008) 577–586.
[4] J.S. Jurvelin, M.D. Buschmann, E.B. Hunziker, Mechanical anisotropy of the human knee articular cartilage in compression, Proc. Inst. Mech. Eng. H. 217 (2003) 215–219.
[5] N.L. Nerurkar, D.M. Elliott, R.L. Mauck, Mechanical design criteria for intervertebral disc tissue engineering, J. Biomech. 43 (2010) 1017–1030.
[6] A.C. Jayasuriya, S. Ghosh, J.I. Scheinbeim, V. Lubkin, G. Bennett, P. Kramer, A study of piezoelectric and mechanical anisotropies of the human cornea, Biosens. Bioelectron. 18 (2003) 381–387.
[7] H. Zhang, A.I. Cooper, Aligned porous structures by directional freezing, Adv. Mater 19 (2007) 1529–1533.
[8] H. Zhang, I. Hussain, M. Brust, M.F. Butler, S.P. Rannard, A.I. Cooper, Aligned two-and three-dimensional structures by directional freezing of polymers and nanoparticles, Nat. Mater 4 (2005) 787–793.
[9] L.E. Millon, H. Mohammadi, W.K. Wan, Anisotropic polyvinyl alcohol hydrogel for cardiovascular applications, J. Biomed. Mat. Res. B Appl. Biomater. 79 (2006) 305–311.
[10] W. Wan, A.D. Bannerman, L. Yang, H. Mak, Poly (vinyl alcohol) cryogels for biomedical applications, Adv. Polym. Sci. 263 (2014) 283–321.
[11] S. Chatelin, M. Bernal, T. Deffieux, C. Papadacci, P. Flaud, A. Nahas, C. Boccara,

J.L. Gennisson, M. Tanter, M. Pernot, Anisotropic polyvinyl alcohol hydrogel phantom for shear wave elastography in fibrous biological soft tissue: a multimodality characterization, Phys. Med. Biol. 59 (2014) 6923–6940.
[12] C.M. Voge, M. Kariolis, R.A. MacDonald, J.P. Stegemann, Directional conductivity in SWNT-collagen-fibrin composite biomaterials through strain-induced matrix alignment, J. Biomed. Mat. Res. A 86 (2008) 269–277.
[13] A. Osorio-Madrazo, M. Eder, M. Rueggeberg, J.K. Pandey, M.J. Harrington, Y. Nishiyama, J.L. Putaux, C. Rochas, I. Burgert, Reorientation of cellulose nanowhiskers in agarose hydrogels under tensile loading, Biomacromolecules 13 (2012) 850–856.
[14] M.C. Swan, D.G. Bucknall, T.E. Goodacre, J.T. Czernuszka, Synthesis and properties of a novel anisotropic self-inflating hydrogel tissue expander, Acta Biomater. 7 (2011) 1126–1132.
[15] W. Yang, H. Furukawa, J.P. Gong, Highly extensible double-network gels with self-assembling anisotropic structure, Adv. Mater 20 (2008) 4499–4503.
[16] M. Haque, G. Kamita, T. Kurokawa, K. Tsujii, J.P. Gong, Unidirectional alignment of lamellar bilayer in hydrogel: one-dimensional swelling, anisotropic modulus, and stress/strain tunable structural color, Adv. Mater 22 (2010) 5110–5114.
[17] X. Pei, T. Zan, H. Li, Y. Chen, L. Shi, Z. Zhang, Pure anisotropic hydrogel with an inherent chiral internal structure based on the chiral nematic liquid crystal phase of rodlike viruses, ACS Macro Lett. 4 (2015) 1215–1219.
[18] S. Ahadian, J. Ramón-Azcón, M. Estili, X. Liang, S. Ostrovidov, H. Shiku, M. Ramalingam, K. Nakajima, Y. Sakka, H. Bae, T. Matsue, Hybrid hydrogels containing vertically aligned carbon nanotubes with anisotropic electrical conductivity for muscle myofiber fabrication, Sci. Rep. 4 (2014) 4271.
[19] K.J. Walker, S.V. Madihally, Anisotropic temperature sensitive chitosan-based injectable hydrogels mimicking cartilage matrix, J. Biomed. Mat. Res. B Appl. Biomater. 103 (2015) 1149–1160.
[20] L.A. Hockaday, K.H. Kang, N.W. Colangelo, P.Y. Cheung, B. Duan, E. Malone, J. Wu, L.N. Girardi, L.J. Bonassar, H. Lipson, C.C. Chu, Rapid 3D printing of anatomically accurate and mechanically heterogeneous aortic valve hydrogel scaffolds, Biofabrication 4 (2012) 035005.
[21] L. Zhang, J. Zhao, J. Zhu, C. He, H. Wang, Anisotropic tough poly (vinyl alcohol) hydrogels, Soft Matter 8 (2012) 10439–10447.
[22] H.M. Tong, I. Noda, C.C. Gryte, Formation of anisotropic ice-agar composites by directional freezing, Colloid Polym. Sci. 262 (1984) 589–595.
[23] F. Yokoyama, E.C. Achife, J. Momoda, K. Shimamura, K. Monobe, Morphology of optically anisotropic agarose hydrogel prepared by directional freezing, Colloid Polym. Sci. 268 (1990) 552–558.
[24] N.W. Meghri, A.E. Donius, B.W. Riblett, E.J. Martin, A.M. Clyne, U.G.K. Wegst, Directionally solidified biopolymer scaffolds: mechanical properties and endothelial cell responses, JOM 62 (2010) 71–75.
[25] X. Qi, J. Ye, Y. Wang, Alginate/poly (lactic-co-glycolic acid)/calcium phosphate cement scaffold with oriented pore structure for bone tissue engineering, J. Biomed. Mater Res. A 89 (2009) 980–987.
[26] N.L. Francis, P.M. Hunger, A.E. Donius, B.W. Riblett, A. Zavaliangos, U.G. Wegst, M.A. Wheatley, An ice-templated, linearly aligned chitosan-alginate scaffold for neural tissue engineering, J. Biomed. Mater Res. A 101 (2013) 3493–3503.
[27] S.R. Caliari, B.A. Harley, The effect of anisotropic collagen-GAG scaffolds and growth factor supplementation on tendon cell recruitment, alignment, and metabolic activity, Biomaterials 32 (2011) 5330–5340.
[28] X. Wu, Y. Liu, X. Li, P. Wen, Y. Zhang, Y. Long, X. Wang, Y. Guo, F. Xing, J. Gao, Preparation of aligned porous gelatin scaffolds by unidirectional freeze-drying method, Acta Biomater. 6 (2010) 1167–1177.
[29] J. Guan, D. Porter, K. Tian, Z. Shao, X. Chen, Morphology and mechanical properties of soy protein scaffolds made by directional freezing, J. Appl. Polym. Sci. 118 (2010) 1658–1665.
[30] M.C. Asuncion, J.C. Goh, S.L. Toh, Anisotropic silk fibroin/gelatin scaffolds from unidirectional freezing, Mat. Sci. Eng. C Mat. Biol. Appl. 67 (2016) 646–656.
[31] Q. Zhang, Y. Zhao, S. Yan, Y. Yang, H. Zhao, M. Li, S. Lu, D.L. Kaplan, Preparation of uniaxial multichannel silk fibroin scaffolds for guiding primary neurons, Acta Biomater. 8 (2012) 2628–2638.
[32] O. Okay, V.I. Lozinsky, Synthesis and structure–property relationships of cryogels, Adv. Polym. Sci. 263 (2014) 103–157.
[33] V.I. Lozinsky, O. Okay, Basic principles of cryotropic gelation, Adv. Polym. Sci. 263 (2014) 49–101.
[34] S. Dogu, O. Okay, Tough Organogels Based on Polyisobutylene with Aligned Porous Structures Polymer, vol. 49, 2008, pp. 4626–4634.
[35] M. Chen, J. Zhu, G. Qi, C. He, H. Wang, Anisotropic hydrogels fabricated with directional freezing and radiation-induced polymerization and crosslinking method, Mat. Lett. 89 (2012) 104–107.
[36] J. Wu, Q. Zhao, J. Sun, Q. Zhou, Preparation of poly (ethylene glycol) aligned porous cryogels using a unidirectional freezing technique, Soft Matter 8 (2012) 3620–3626.
[37] M. Barrow, A. Eltmimi, A. Ahmed, P. Myers, H. Zhang, Frozen polymerization for aligned porous structures with enhanced mechanical stability, conductivity, and as stationary phase for HPLC, J. Mat. Chem. 22 (2012) 11615–11620.
[38] D. Zhao, J. Zhu, Z. Zhu, G. Song, H. Wang, Anisotropic hierarchical porous hydrogels with unique water loss/absorption and mechanical properties, RSC Adv. 4 (2014) 30308–30314.
[39] R.D. Arrua, E.F. Hilder, Highly ordered monolithic structures by directional freezing and UV-initiated cryopolymerisation. Evaluation as stationary phases in high performance liquid chromatography, RSC Adv. 5 (2015) 71131–71138.
[40] M. Chau, K.J. De France, B. Kopera, V.R. Machado, S. Rosenfeldt, L. Reyes, K.J. Chan, S. Förster, E.D. Cranston, T. Hoare, E. Kumacheva, Composite hydrogels with tunable anisotropic morphologies and mechanical properties, Chem. Mater 28 (2016) 3406–3415.
[41] C. Vepari, D.L. Kaplan, Silk as a biomaterial, Prog. Polym. Sci. 32 (2007) 991–1007.
[42] F. Vollrath, D. Porter, Silks as ancient models for modern polymers, Polymer 50 (2009) 5623–5632.
[43] J.G. Hardy, L.M. Romer, T.R. Scheibel, Polymeric materials based on silk proteins, Polymer 49 (2008) 4309–4327.
[44] U.J. Kim, J. Park, C. Li, H.J. Jin, R. Valluzzi, D.L. Kaplan, Structure and properties of silk hydrogels, Biomacromolecules 5 (2004) 786–792.
[45] A. Matsumoto, J. Chen, A.L. Collette, U.J. Kim, G.H. Altman, P. Cebe, D.L. Kaplan, Mechanisms of silk fibroin sol-gel transitions, J. Phys. Chem. B 110 (2006) 21630–21638.
[46] H.J. Jin, D.L. Kaplan, Mechanism of silk processing in insects and spiders, Nature 424 (2003) 1057–1061.
[47] C. Dicko, J.M. Kenney, D. Knight, F. Vollrath, Transition to a beta-sheet-rich structure in spidroin in vitro: the effects of pH and cations, Biochemistry 43 (2004) 14080–14087.
[48] Karakutuk, F. Ak, O. Okay, Diepoxide-triggered conformational transition of silk fibroin: formation of hydrogels, Biomacromolecules 13 (2012) 1122–1128.
[49] T. Yucel, P. Cebe, D.L. Kaplan, Vortex-induced injectable silk fibroin hydrogels, Biophys. J. 97 (2009) 2044–2050.
[50] E. Servoli, D. Maniglio, A. Motta, C. Migliaresi, Folding and assembly of fibroin driven by an AC electric field: effects on film properties, Macromol. Biosci. 8 (2008) 827–835.
[51] X. Chen, D.P. Knight, Z. Shao, F. Vollrath, Conformation transition in silk protein films monitored by time-resolved Fourier transform infrared spectroscopy: effect of potassium ions on Nephila spidroin films, Biochemistry 41 (2002) 14944–14950.
[52] C. Mo, C. Holland, D. Porter, Z. Shao, F. Vollrath, Concentration state dependence of the rheological and structural properties of reconstituted silk, Biomacromolecules 10 (2009) 2724–2728.
[53] A. Argun, V. Can, U. Altun, O. Okay, Non-ionic double and triple network hydrogels of high mechanical strength, Macromolecules 47 (2014) 6430–6440.
[54] X. Hu, D. Kaplan, P. Cebe, Effect of water on the thermal properties of silk fibroin, Thermochim. Acta 461 (2007) 137–144.
[55] F. Ak, Z. Oztoprak, I. Karakutuk, O. Okay, Macroporous silk fibroin cryogels, Biomacromolecules 14 (2013) 719–727.
[56] O. Okay, Macroporous copolymer networks, Prog. Polym. Sci. 25 (2000) 711–779.
[57] S.J. Park, K.Y. Lee, W.S. Ha, S.Y. Park, Structural changes and their effect on mechanical properties of silk fibroin/chitosan blends, J. Appl. Polym. Sci. 74 (1999) 2571–2575.
[58] M.F. Butler, Instability formation and directional dendritic growth of ice studied by optical interferometry, Cryst. Growth Des. 1 (2001) 213–223.